Application of a 2D segregation-dispersion model to describe binary and multi-component size classification in a Reflux Classifier

N.H. Syed, K.P. Galvin, R. Moreno-Atanasio*

Centre for Advanced Particle Processing and Transport, Chemical Engineering Department, the University of Newcastle, NSW, Australia

*Corresponding author. Email: roberto.moreno-atanasio@newcastle.edu.au

Abstract

A 2D segregation-dispersion model was utilized to study the transport mechanism of particle species in the Reflux Classifier (RC) with a wide channel spacing. The main objective was to study size classification and describe the internal state of the system under continuous process conditions with changing variables such as fluidization velocity, underflow rate and solids throughput. Moreover, the Richardson and Zaki hindered settling model was incorporated into the 2D model to study the separation of particle species based on differences in their settling velocities. A set of simulations was performed for binary and multicomponent mixtures, having a density equal to 2490 kg/m^3 in both cases. For the binary mixture, particle species of size 200 and 300 μm were used, while for the multicomponent mixture eight particle species with sizes between 49 and 421 μm were selected. The partition curves obtained from the model predictions were successfully validated with published experimental results. The separation performance of the RC was characterised by analysing how the imperfection and the d_{50} values changed with the process variables. Furthermore, the simulation data were used for the first time to demonstrate the concentration distribution of the individual solid particle species in the fluidization and inclined sections of the RC. This study showed that the particle species with sizes closer to the d_{50} values had a larger presence in both the vertical and inclined sections of the RC. Thus, the total concentration inside the RC mainly consisted of those particle species.

Keywords: Beneficiation; Fluidization; Hindered settling; Inclined channel; Slip velocity; Size classification; Classifier

1. Introduction

The separation of solid particles on the basis of size and density has been an important area of research due to its direct applications in a wide range of industries including beneficiation in the mining industry, and classification in the construction and wastewater treatment industries (Di Felice, 1995; Doroodchi et al., 2006; Horio, 2010). In mineral processing, the separation of particle species of different sizes and densities is often carried out using liquid fluidized beds (Rasul, 2000; Epstein, 2005; Mukherjee et al., 2009) and the Reflux Classifier (Galvin et al., 2005, 2010; Amariei et al., 2014; Hunter et al., 2016).

The Reflux Classifier (RC) consists of a set of parallel inclined channels above a fluidized bed (Nguyentranlam and Galvin, 2001; Galvin and Nguyentranlam, 2002). The fluidization section segregates particle species in a similar way to that observed in liquid fluidized beds while the inclined channels work on the principle of the Boycott Effect (Boycott, 1920) by providing a large effective settling area, hence promoting strong levels of particle segregation (Nguyentranlam and Galvin, 2001; Galvin and Nguyentranlam, 2002; Galvin et al., 2010). A 2D schematic representation of the RC is shown in Fig. 1.

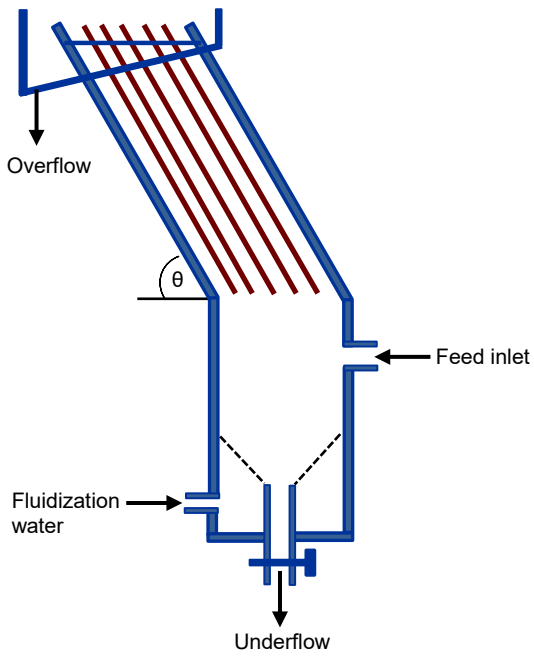

Fig. 1. 2D schematic diagram of the Reflux Classifier.

Different modelling approaches such as Computational Fluid Dynamics (CFD) (Anderson and Jackson, 1967; Cornelissen et al., 2007; Huang, 2011), CFD-DEM (Discrete Element Method) (Zhu et al., 2008, Cornelissen et al., 2007; Khan et al., 2014) and convection-diffusion (segregation-dispersion) equations (Kennedy and Bretton, 1966; Juma and Richardson, 1983; Asif and Petersen, 1993; Patel et al., 2008; Syed et al., 2018) have been used to study the transport mechanism of solid particles in liquid fluidized beds and the RC.

Kennedy and Bretton (1966) were the first researchers to propose a segregation-dispersion model (Asif and Petersen, 1993) to investigate the transport mechanism of binary particle species in liquid fluidized beds under batch process conditions, given as,

$$J = \phi_i v_{p,i} = -D_i \frac{\partial \phi_i}{\partial y} + \phi_i v_{seg,i} \quad (1)$$

where J is the net flux, v_p is the particle velocity relative to the vessel, D is the dispersion coefficient of particle species i, y is the axial direction of the vessel, v_{seg} is the segregation velocity, $\phi_i v_{seg,i}$ is the segregation flux, $D_i \frac{\partial \phi_i}{\partial y}$ is the diffusion flux and $\phi_i v_{p,i}$ is the particle flux.

In this model, the inherent complexity of a multicomponent process is reduced to a remarkably simple theoretical framework through the introduction of two contributions, segregation and dispersion fluxes, which describe particle transport. The segregation-dispersion model of Kennedy and Bretton (1966) has become the basis for most of the segregation-dispersion models proposed since then (Ramirez and Galvin, 2005).

A significant amount of work has been carried out describing segregation and dispersion phenomena in liquid fluidized beds for binary mixtures under batch process conditions (Kennedy and Bretton, 1966; Juma and Richardson, 1983; Asif, 1997; Ramirez and Galvin, 2005). However, there are far fewer studies focussed on the segregation of binary and multicomponent systems under continuous process conditions in liquid fluidized beds and the RC. Recently, Syed et al. (2018) modified the segregation-dispersion model of Kennedy and Bretton (1966) and proposed a comprehensive 2D computational segregation-dispersion model for the RC.

Syed et al. (2018) utilized the 2D segregation-dispersion model to study the continuous separation of a complex multicomponent mixture comprising 42 particle species of different densities and sizes at the same time. In the former work the focus was on the separation of the particles according to their density. The hindered settling model proposed by Asif (1997) was incorporated as a constitutive model into the 2D segregation-dispersion equation, removing the explicit dependency of settling processes on particle size. This work (Syed et al. 2018) also incorporated a new laminar-shear mechanism that leads to the selective shear-induced lift of the low-density particles within the inclined channels, again enhancing the separation performance of the RC.

The purpose of this paper is to study the opposing problem to that investigated in Syed et al. (2018), i.e. the size classification of particles of a single density in the RC under continuous processing conditions. With particle size classification, it is appropriate to reduce the role of shear-induced lift, by reducing the volumetric flow rate and/or by using a wider channel spacing. In the present work a constant dispersion coefficient was applied, effectively switching off the laminar-shear mechanism. In the 2D model, the Richardson and Zaki slip velocity model was incorporated to describe the hindered settling. Therefore, coarser species having a higher settling velocity moved towards the base of the RC, while finer species with lower settling velocity moved out via the overflow.

The model predictions have been validated against the published experimental results of Doroodchi et al. (2006), which used experimental conditions that involved relatively little shear-induced lift in the RC due to a wide channel spacing. This study is significant because, for the first time, the internal state of the system, and how this state responds to the changes in the primary operating parameters governing the particle size classification, is revealed. In particular, the 2D segregation-dispersion model of the RC provides a framework in which alternative hindered settling models and dispersion models could be inserted and the transport mechanism of particles within the RC studied.

2. Mathematical modelling

According to Kennedy and Bretton (1966), the segregation-dispersion model describes the net flux of a particle species in terms of the dispersion and segregation fluxes. In a system comprising inclined channels above a fluidized bed, the net flux of a particle species relative to the vessel has x and y components (Syed et al., 2018) due to inclination of the channels, given as,

$$J_{x,i} = \phi_i v_{p\_x,i} = -D_{x,i}\frac{\partial \phi_i}{\partial x} + \phi_i v_{seg\_x,i} \quad (2)$$

$$J_{y,i} = \phi_i v_{p\_y,i} = -D_{y,i}\frac{\partial \phi_i}{\partial y} + \phi_i v_{seg\_y,i} \quad (3)$$

where J_x, J_y, v_{p_x}, v_{p_y}, v_{seg_x}, v_{seg_y}, D_x, D_y, and ϕ_i are the net flux, particle velocity, segregation velocity relative to the vessel, dispersion coefficient and concentration of the particle species i in the x and y directions, respectively. The products of the concentration gradient and the dispersion coefficient, $-D_i\frac{\partial \phi_i}{\partial x}$ and $-D_i\frac{\partial \phi_i}{\partial y}$, are the dispersion fluxes in the x and y directions, respectively. Similarly, the products of the volume fraction and the segregation velocity of the particles species, $\phi_i v_{seg\_x,i}$ and $\phi_i v_{seg\_y,i}$ are the segregation fluxes in the x and y directions, respectively.

For a continuous process, it is necessary to consider the solid and liquid entering the system through the inlet and leaving the system as underflow and overflow. Therefore, the total volume flux, v_n, balance through the system just above the feed inlet is given as,

$$v_n = v_{fs} + J_f - J_u = v_f\phi_f + \sum \phi_i v_{p,i} \quad (4)$$

Similarly, below the feed point the total volume flux is given as,

$$v_n = v_{fs} - J_u = v_f\phi_f + \sum \phi_i v_{p,i} \quad (5)$$

where, v_{fs} is the superficial fluidization velocity, v_f the interstitial fluid velocity, J_f is the feed flux, J_u is the underflow flux and ϕ_f is the voidage.

The segregation fluxes are written as a function of the slip velocities in the respective directions. Now the segregation velocity has x and y components and is given in terms

of the corresponding sum of the particle slip and interstitial fluid velocities. The equations for the components of the segregation velocity become,

$$v_{seg\_x,i} = v_{slip\_x,i} + v_{f\_x} \quad (6)$$

$$v_{seg\_y,i} = v_{slip\_y,i} + v_{f\_y} \quad (7)$$

where $v_{slip\_x,i}$ and $v_{slip\_y,i}$ are the slip velocities of the particle species relative to the fluid in the x and y directions, respectively. Likewise, v_{f_x} and v_{f_y} are the interstitial fluid velocities in the x and y directions, respectively.

The x and y components of the slip velocity were calculated using the Richardson and Zaki (1954) equation represented as,

$$v_{slip\_x,i} = \left[v_{t,i}(1-\phi_t)^{n_i-1}\right]\cos\theta \quad (8)$$

$$v_{slip\_y,i} = \left[v_{t,i}(1-\phi_t)^{n_i-1}\right]\sin\theta \quad (9)$$

where $v_{t,i}$, ϕ_t and n are the terminal velocity, total solid concentration (v/v) and the Richardson and Zaki (1954) exponent, respectively.

The net flow (solid particles plus water) within the inclined channel was considered to have a parabolic profile. Therefore, the superficial velocity, v_o, in the inclined channel is given as,

$$v_o = \frac{6v_n x_p}{z}\left(1-\frac{x_p}{z}\right) \quad (10)$$

where z is the channel spacing and x_p is the distance, within the inclined channel, from the particle to the channel wall.

At steady state the interstitial fluid velocity in the fluidization section is obtained using Eq. (4) and (5), whereas within the inclined channel, parallel to the plane (y direction) the interstitial fluid velocity is given as,

$$v_{f\_y} = \frac{(v_o - \sum\phi_i v_{p\_y,i})}{(1 - \sum\phi_i)} \quad (11)$$

The settling of particle species normal to the plane within the inclined channel was considered to be similar to that of batch settling. Thus, the interstitial fluid velocity normal to the plane (x direction) was obtained as,

$$0 = v_{f\_x}\,\phi_f + \sum \phi_i v_{p\_x,i} \tag{12}$$

Therefore,

$$v_{f\_x} = \frac{-\sum \phi_i v_{p\_x,i}}{\phi_f} \tag{13}$$

The boundary condition at the base of the system was equal to the underflow flux moving out from the system. Similarly, at the top of the system a free boundary condition was assumed, and the dispersion flux was taken as zero at the top of the system. The boundary conditions for the 2D segregation-dispersion model are given as:

$$y = y_{max} \qquad \frac{\partial \phi_i}{\partial y} = 0 \tag{14}$$

$$y = 0 \qquad J_{y,i} = J_u \tag{15}$$

2.1. Particle terminal velocity and partition curve

The particle Reynolds number, Re_t, and the Richardson and Zaki (1954) exponent, n, were calculated using the Zigrang and Sylvester (1981) equation (Syed et al., 2018) and the correlations of Richardson and Zaki (1954), respectively.

Size partition curves were produced from the data generated from the simulations. The size partition curves describe the probability of the different size particles reporting to either the underflow or overflow. For the partition curve, the d_{50} indicates the size of a particle species with a 50% probability of reporting either to the underflow or overflow (Syed et al. 2018, Syed, 2017).

2.2. Simulation parameters

The fluidization velocity, feed rate and underflow rate were applied from the beginning of the simulations. In modelling the Reflux Classifier (RC), only one inclined channel was used, with the angle of inclination with respect to the horizontal set at 70^0. The height, H, and width, w, of the fluidization section was taken as 1 m and 0.006 m, respectively. Similarly, the length of the inclined channel was taken as 1 m and the width i.e. channel spacing $wsin\theta$. The feed inlet point was located at a height of 0.8 m (i.e. shell 80) while the inclined channel started from 1 m (i.e. shell 101).

In this study, a constant value of the dispersion coefficient equal to 0.00030 m^2/s in the x and y directions was applied within the computational domain of the RC. This value of the dispersion coefficient was identical to the value used in the previous study by Syed et al. (2018), although the process conditions were completely different. The value of the dispersion coefficient, selected as a fitting parameter (independent of the particle size and shear rate), was within the typical range found in the literature (Juma and Richardson, 1983; Asif and Petersen, 1993; Patel et al., 2008; Syed et al. 2018).

The 2D segregation-dispersion model was used to study the size classification of binary and multicomponent mixtures. The binary mixture consisted of particle species of diameters 200 and 300 μm having an identical density 2490 kg/m^3 in the RC. The properties of the solid particles are shown in Table 1.

Table 1: Properties of binary particle species.

Particle density (kg/m^3)	Particle size (μm)	Particle size (m)	Terminal velocity (m/s)	Richardson & Zaki Exponent n
2490	200	0.00020	0.022	4.31
2490	300	0.00030	0.035	4.19

During the simulations, an underflow flux of 0.00020 m^3/m^2s was maintained while the solid flux in the feed stream was kept at 0.00015 m^3/m^2s for each particle species. The water flux in the feed stream was 0.0045 m^3/m^2s making a total flux (solids plus water) of 0.0048 m^3/m^2s entering the system.

Similarly, in the multicomponent mixture a total number of eight particle species having the same density but different sizes were used in the simulations. The density was

taken to be equal to 2490 kg/m^3, with the particle diameter ranging from 49 to 421 μm. A total feed flux of 0.0048 m^3/m^{2}s with a solid flux of 0.00030 m^3/m^{2}s were used. The feed conditions and process variables were taken according to the experimental conditions of Doroodchi et al. (2006). Furthermore, the model predictions were validated with the published experimental result of Doroodchi et al. (2006). The properties of the particle species considered in the simulations are presented in Table 2.

Table 2: Properties of particle species density equal to 2490 kg/m^3.

Particle size (μm)	Terminal settling velocity (m/s)	Exponent n
49	0.0019	4.81
69	0.0032	4.81
97	0.0076	4.73
137	0.014	4.47
164	0.017	4.30
195	0.022	4.32
274	0.032	4.21
421	0.052	4.16

2.4. Model Implementation

The computational domain of the Reflux Classifier (RC) including the fluidized and inclined sections was discretized into equally spaced shells and elements in the x and y directions, respectively, as shown in Fig. 2. The system was divided into 200 shells and 21 elements. The elements were numbered from 1 to 21, commencing from the element closest to the upward facing wall of the inclined surface.

The segregation velocities in the x and y directions were calculated using equations (6) and (7). For a given particles species *i*, if the segregation flux is positive, then a volume of material equal to $\phi_i v_{seg\_y,i} A \Delta t$ will move from the shell n to the shell n+1. In contrast, if the segregation flux of a particle species *i* is negative, then a volume equal to $\phi_i v_{seg\_y,i} A \Delta t$ will move downwards from the shell n to the shell n-1 (Patel et al., 2008; Syed et al., 2018).

The dispersion flux depends on the concentration gradient. If the concentration gradient has a negative value, then the dispersion flux becomes positive and particle species *i* moves from the current shell to the upper shell. In contrast, for a positive gradient, the dispersion flux becomes negative and particle species *i* moves in the axial direction from the upper shell to the current shell. The movement of material in the x direction takes place from one element to another following the same algorithm described for the y direction (Patel et al., 2008; Syed et al., 2018).

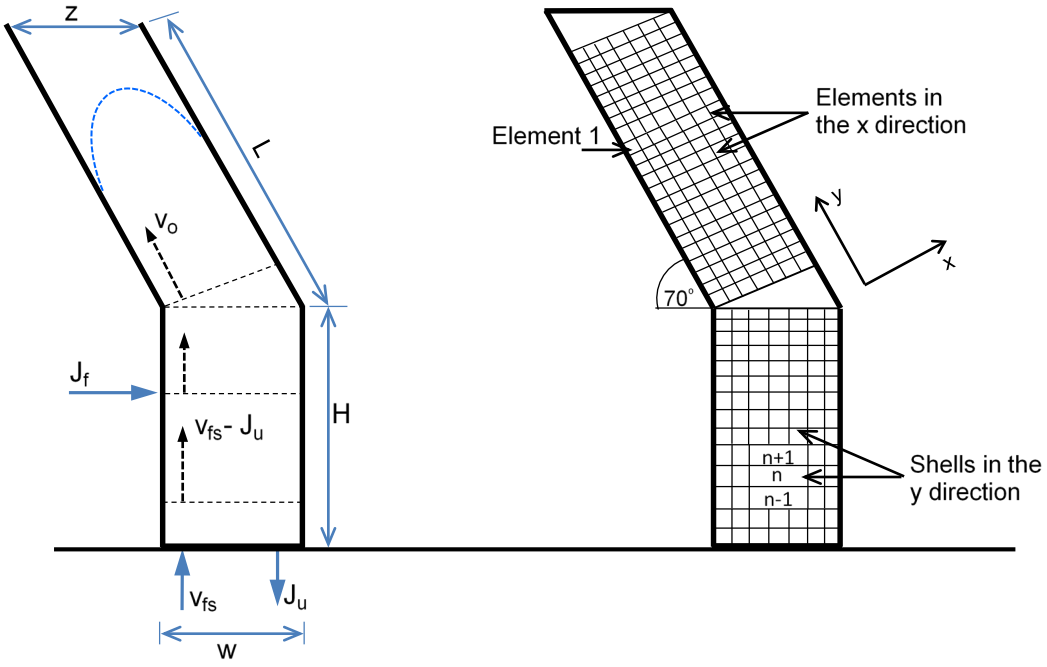

Fig. 2: Schematic diagram of the computational domain of the Reflux Classifier showing the flux movement, shells in the y direction and elements in the x direction.

3. Results and Discussion

Simulations were carried out for binary and multicomponent mixtures using the 2D segregation-dispersion model. In the 2D model, the segregation and dispersion fluxes are two opposing mechanisms and together define the movement of the solid particles within the system. The segregation term describes the separation tendency of the particle species whereas the dispersion term governs the random mixing of the particle species, both having a fundamental hydrodynamic origin. If the value of the dispersion coefficient is very high, the particles become mixed thus limiting any observed

segregation (Kennedy and Bretton, 1966; Juma and Richardson, 1983). In contrast, if the value of the dispersion coefficient is relatively low, segregation is free to occur.

In the 2D model, the segregation flux had x and y components. In the fluidization section of the RC, the x component was zero while the y component described the movement of the particle species. The particle species having a negative segregation velocity moved downwards, whereas, the particle species having a positive segregation velocity moved upwards relative to the container. Within the inclined channels, the x and y components both contributed to the movement of the particle species. The particle species that settled within the inclined sections had a relatively high segregation velocity in the x direction. Similarly, the dispersion flux had x and y components in the fluidization section of the RC. The x component helped in dispersing the particle species across the width of the fluidization section. In contrast, the y component of the dispersion flux contributed to the transport in the axial direction. Likewise, the two components of the dispersion contributed to the normal and parallel directions within the inclined section of the RC. The dispersion flux was the source of mixing and resistance to separation within the RC.

3.1. Model predictions for a binary mixture

Simulations were performed using the binary particle species shown in Table 1. The particle species segregated into two mono-component zones, as shown in Fig. 3a-d. At the steady state, reached in 900 s, coarser particle species due to their higher settling velocity and thus negative segregation velocity moved downwards and formed a higher concentration zone at the base of the system. These particles continuously discharged from the system in the underflow. In contrast, finer particle species, due to their lower settling velocity had a positive segregation velocity and moved upwards with the hydraulic conveying. These finer particle species entered the inclined section of the RC and moved out in the overflow. Fig. 3a-d shows the concentration distribution of particle species as a function of height for the horizontal elements 1, 6, 11 and 21 at steady state. The concentration distributions of coarser and finer particle species are represented by the blue (dashed-dotted) and black (continuous) curves, respectively.

The model predictions in Fig. 3a-d show that the concentration distribution of particle species was similar in all elements of the fluidization section (elements 1-21) of the

RC. However, within the inclined channel, the concentration distribution changed across the channel width in each element. At steady state, the system reached a maximum concentration of 0.17 (v/v) in the fluidization section of the RC. In this section, the coarser species had a higher concentration, whereas the finer species had almost zero concentration suggesting that the finer species did not discharge in the underflow. The model also predicted a mixing zone (between 0.6 to 1 mm height) in the fluidization section of the RC where the presence of both species is visible.

In Fig. 3a, within the inclined section of the RC, the concentration of finer species in element 1 (element closest to the upward facing wall of the inclined channel) was higher (0.044) than for the coarser species. The presence of the coarser species was almost zero within the inclined section suggesting that these species stayed mainly in the fluidization section of the RC. Furthermore, in Fig. 3(b, c &d), in the elements 6, 11 and 21 the concentration of the finer particle species decreased gradually from the value of 0.044 (Fig. 3a) to 0.039 (Fig. 3d) because the particles were settling while moving through the inclined channel.

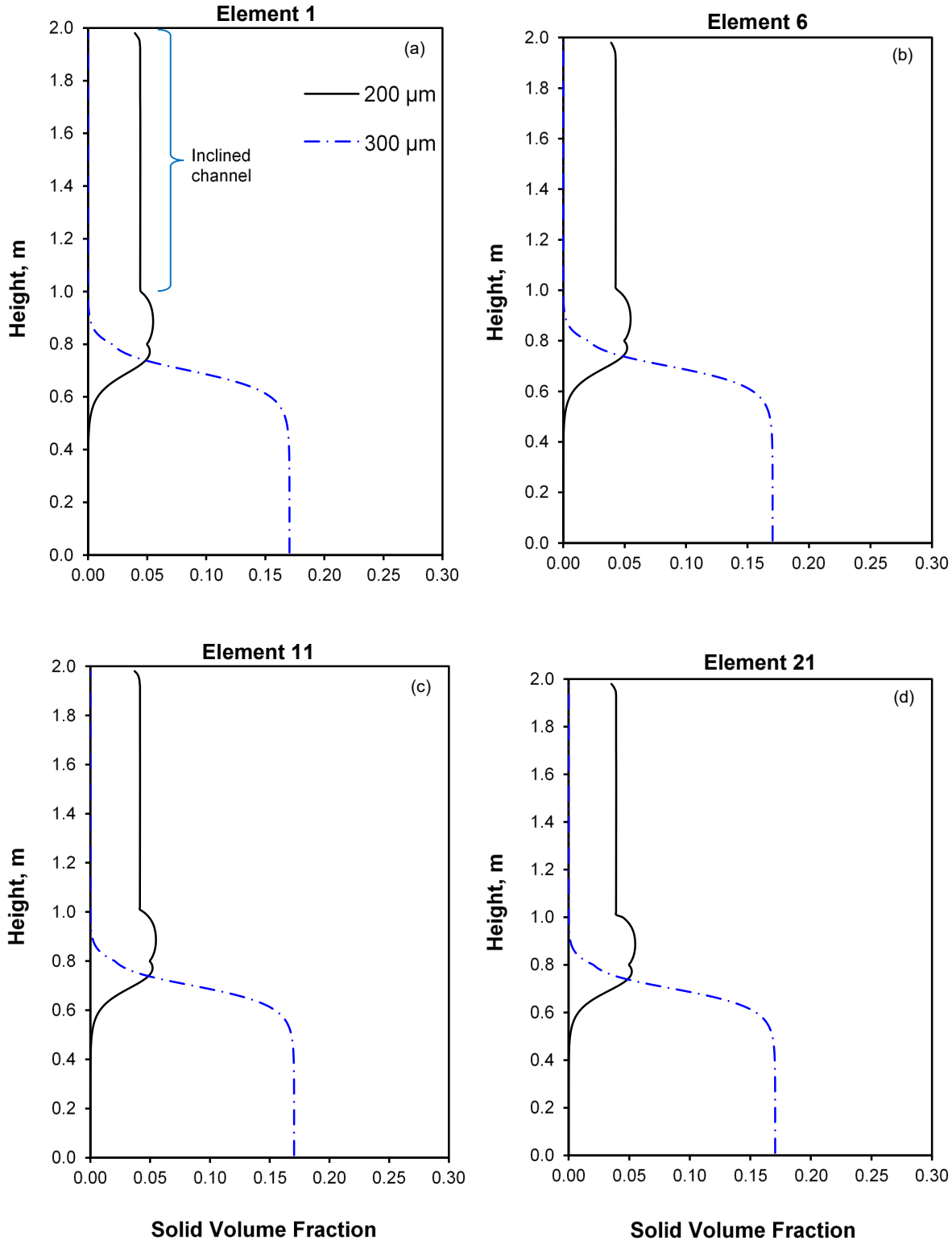

Fig. 3(a-d): Concentration distribution across the system height for a binary mixture at steady state in the Reflux Classifier for different elements: (a) element 1; (b) element 6; (c) element 11; (d) element 21.

Fig. 4a-b presents the dynamic response of the concentration distribution as a function of height in the RC at different times. Fig. 4a illustrates the settling behaviour of the finer particle species with time in element 1. The figure shows that the concentration of the finer particle species was higher initially at 200 s in the fluidization section of the RC. However, as time passed, i.e. at 400 s, 800 s, and 1000 s, the concentration of finer particle species started to decrease, whereas the concentration of coarser particle species increased within the vertical section. This is because the finer particle species started moving upwards and entered the inclined section. Similarly, within the inclined section, at 200 s the concentration of finer particle species was low but gradually increased with time and reached a maximum value of 0.044.

Fig. 4b shows the dynamic response of the concentration distribution of the coarser particle species in the RC. At 200 s, the concentration of the coarser particle species was low because the particles just started to move into the RC. The profile of the concentration distribution changed with time as coarser particles started to accumulate near the base. The concentration of coarser particle species gradually increased at time 400 s and reached a maximum value of 0.17 at 1000 s. However, within the inclined section, the concentration of coarser particle species was almost zero suggesting that the fluidization and feed fluxes were not sufficient to transport these particles to the inclined section.

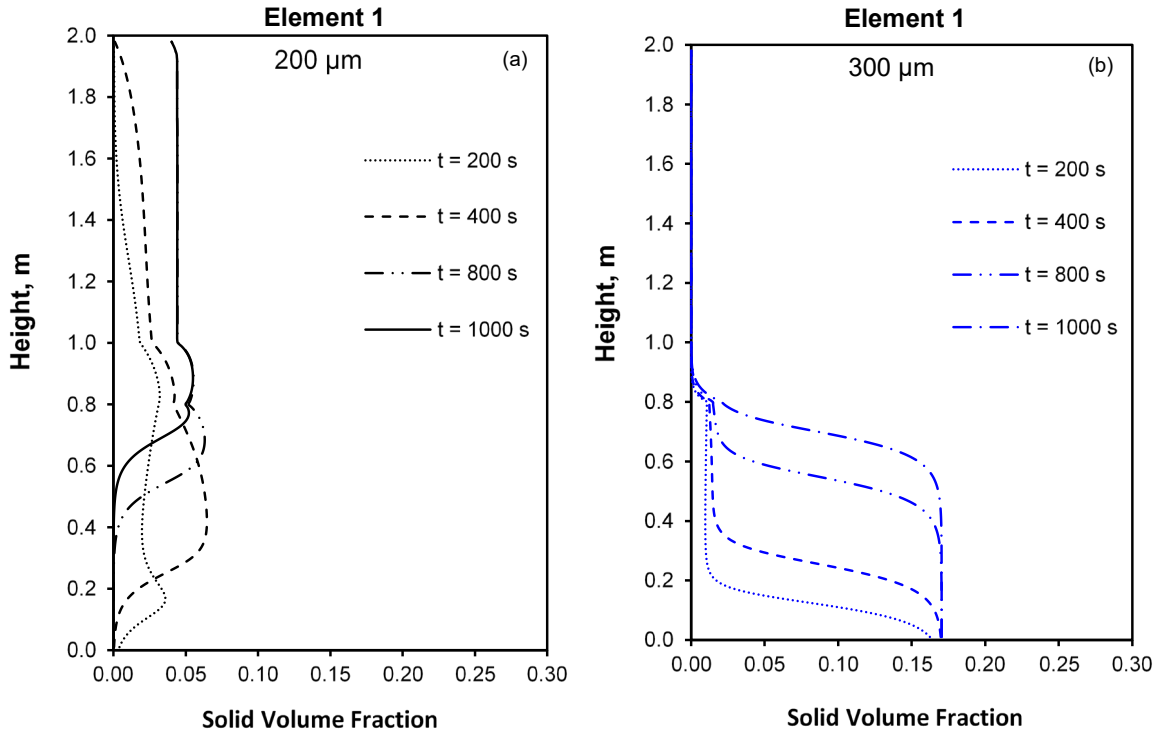

Fig. 4(a-b): Concentration distribution versus height for a binary mixture at different times: (a) element 1 for 200 µm; (b) element 1 for 300 µm.

3.2. Model predictions for a multicomponent mixture

The 2D model was utilized to study the size classification and influence of variables such as fluidization velocity, underflow rate and solids throughput on the separation performance of the Reflux Classifier (RC) by assessing variations in the imperfection (Doroodchi et al., 2006) and the d_{50} values. The simulation results corresponding to the steady state for a multicomponent system presented in Table 2, have been shown and discussed in this section.

3.2.1. Influence of fluidization velocity

Simulations were performed to investigate the segregation of the particle species at two different fluidization velocities, 0.016 and 0.028 m/s. Fig. 5 shows a comparison between the partition curves obtained through the model predictions and the published experimental results of Doroodchi et al. (2006). In the figure, the dashed lines with empty circles and squares represent the experimental results, whereas the continuous lines with filled circles and squares represent the model predictions. The comparison

of model predictions with the experimental results provided a very good agreement demonstrating that the changes in the d_{50} value with fluidization velocity was similar to that observed in the experiments by Doroodchi et al. (2006). The results show that the d_{50} value changed from 150 to 176 μm for the fluidization velocities 0.016 and 0.028 m/s, respectively.

According to the partition curves, the coarser particle species discharged into the underflow while the finer particle species reported to the overflow. The imperfection, *I,* obtained through the model predictions was relatively high, i.e. 0.071, in the case of the higher fluidization velocity. However, at the lower fluidization velocity, the imperfection value was 0.066 indicating that the separation quality improved slightly with decreasing fluidization velocity.

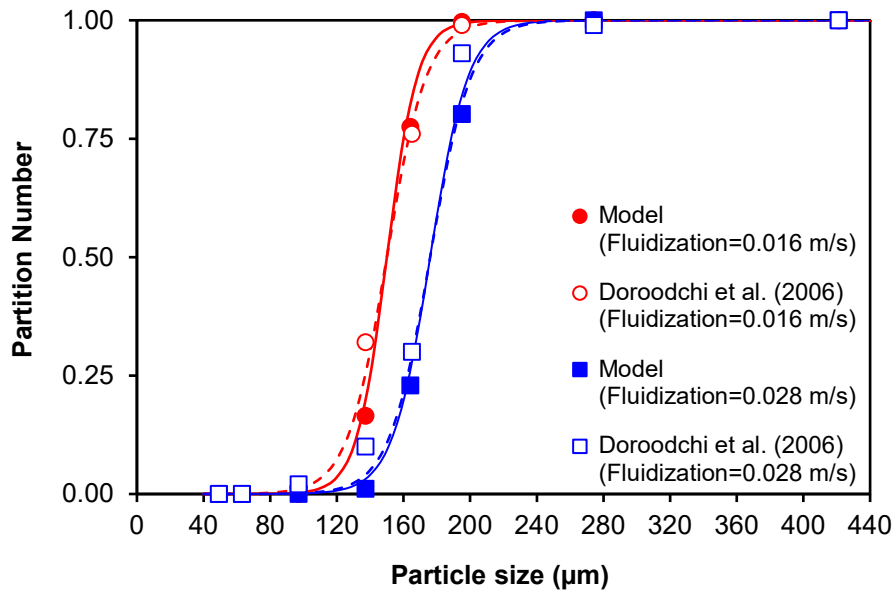

Fig. 5: Partition number versus particle size at the fluidization velocities of 0.016 and 0.028 m/s. Comparison of model predictions with the experimental results of Doroodchi et al. (2006).

3.2.2. Influence of fluidization velocity on the concentration distribution of particle species

Fig. 6a-b illustrates the concentration distribution of individual particle species within the Reflux Classifier (RC) at two different fluidization velocities of 0.016 and 0.028 m/s. For simplicity, only the concentration distributions in element 1 for both cases have been shown. A more detailed representation of the concentration profiles in elements 1, 11 and 21 can be found in Appendix A. In the figure, the profiles of particle species up to 1 m and from 1 m to 2 m height represent the concentration distribution within the fluidization and inclined sections of the RC, respectively.

Fig. 6a shows the concentration distribution with respect to the height of the RC at a fluidization velocity of 0.016 m/s. The concentration profiles of the particle species in the fluidization section show that two of the coarser species (195 and 274 μm) had a higher concentration near the base of the RC (blue and black curves). However, the coarsest particle species of size 421 μm had a near zero concentration at the bottom of the unit suggesting that this particle species completely discharged from the system in the underflow. In contrast, the finer particle species moved upwards due to hydraulic loading. The particle species of size 49 μm and 69 μm completely moved out from the RC. However, the particle species of size 97 μm has shown its presence within the inclined section with a concentration of 2.46×10^{-3} (v/v). Interestingly, the particle species of size 137 and 164 μm have shown their presence in both the fluidization and inclined sections of the RC. These species have sizes closer to the d_{50} which was 150 μm. Therefore, the particle species closest to the d_{50} value had an elevated concentration in the system.

Similarly, Fig. 6b represents the concentration distribution of individual particle species in the RC at a fluidization velocity of 0.028 m/s. At this fluidization velocity, the value of d_{50} shifted to a higher value of 176 μm (Fig. 5). Therefore, the simulations show the presence of the particle species of size 164 and 195 μm in both sections of the RC. In this case, the particle species of size 137 μm were present in the inclined section of the RC with a concentration of 4.34×10^{-3} (v/v), whereas for the lower fluidization velocity these species were present in both the fluidization and inclined sections (red curve). Overall, the variations in the concentration profiles with changing fluidization velocity were consistent with the changes in the d_{50} values.

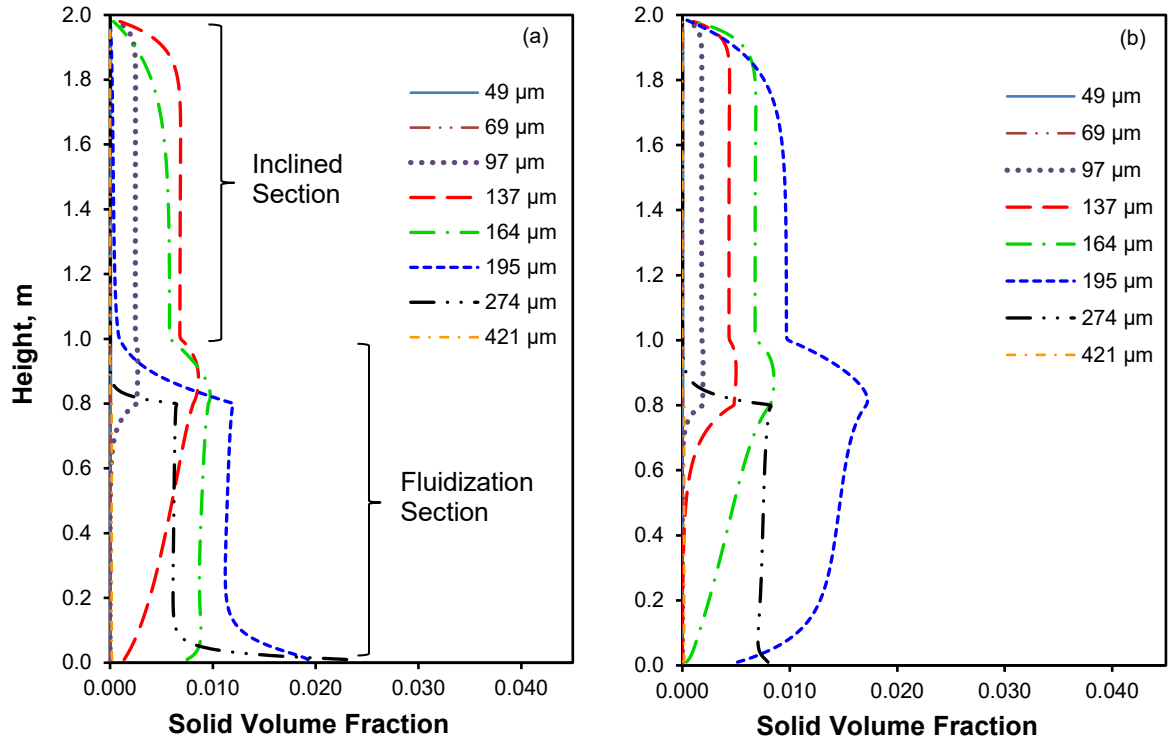

Fig. 6(a-b): Concentration distribution of individual particle species at different fluidization velocities in element 1: (a) 0.016 m/s; (b) 0.028 m/s.

3.2.3. Influence of underflow rate

Simulations were performed to examine the performance of the Reflux Classifier (RC) at three different underflow rates 0.0065, 0.0045 and 0.0025 m^3/m^2s, while keeping the fluidization velocity at 0.016 m/s. Fig. 7 presents the size partition curves corresponding to the three underflow rates used in the simulations. The simulation results show that the value of the d_{50} decreased from 170 to 130 µm as the underflow rate increased from 0.0025 to 0.0065 m^3/m^2s, respectively.

The imperfection was also affected by changes in the underflow rate. The imperfection for the underflow rates of 0.0025 and 0.0045 m^3/m^2s were 0.065 and 0.066, respectively, suggesting a good separation quality. However, at the highest underflow rate (0.0065 m^3/m^2s) the imperfection increased to a value of 0.085 illustrating a poorer separation condition than in the case of 0.0025 m^3/m^2s. This variation in the separation quality was probably due to an increase in the presence of fine particle species that were dragged towards the underflow.

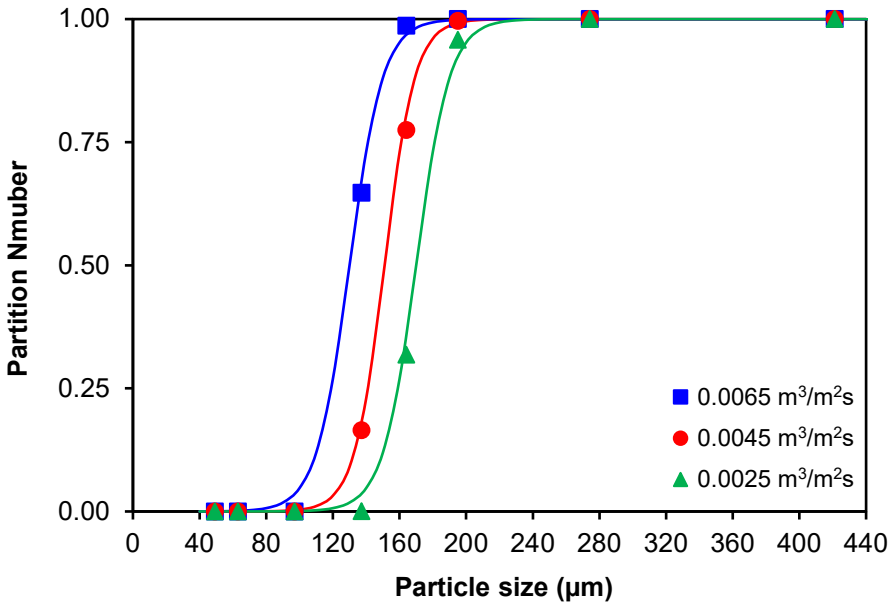

Fig. 7: Partition number versus particle size at different underflow rates.

3.2.4. Influence of underflow rate on concentration distribution

Fig. 8a-b shows the concentration distribution of individual particle species within the Reflux Classifier (RC) at two different underflow rates 0.0025 and 0.0065 m^3/m^2s under steady state conditions. In Fig. 8a, the concentration distribution of individual particle species versus height for the underflow rate 0.0025 m^3/m^2s is shown. The concentration profiles show that the finest and coarsest species moved out from the system completely and, thus, their concentrations were almost zero within the RC. However, the particle species of 97 and 274 μm showed their presence within the system, with the 97 μm species having a larger presence in the inclined section and the 274 μm species in the fluidization section. Furthermore, the particle species with size 137 μm had a relatively low concentration in the fluidization section (at 0.8 to 1 m) compared to its concentration in the inclined section. These particle species, 137 μm, also moved out from the system via the overflow. As the value of the d_{50} for this case was 170 μm (Fig. 7), the particle species of size 164 and 195 μm acted as proxies for the d_{50}. These species had relatively high concentrations in both the fluidization and inclined sections of the RC (green and blue curves).

Fig. 8b shows the concentration distribution of individual particle species versus height for the underflow rate 0.0065 m^3/m^2s. The value of the d_{50}, in this case, was 130 μm (Fig. 7), so the particle species of size 137 μm (red curve) acted as a d_{50} proxy with an

elevated presence in both sections of the RC. A comparison of Figures 8a and 8b shows that the particle species of size 164 and 195 μm were completely discharged in the case of the higher underflow rate (0.0065 m^3/m^2s). Similarly, the particle species of size 97, 137 and 164 μm had comparatively high concentrations in the fluidization section as shown in Fig. 8b. The presence of these finer particle species in the fluidization section explains the poorer separation for an underflow rate of 0.0065 m^3/m^2s (section 3.2.3).

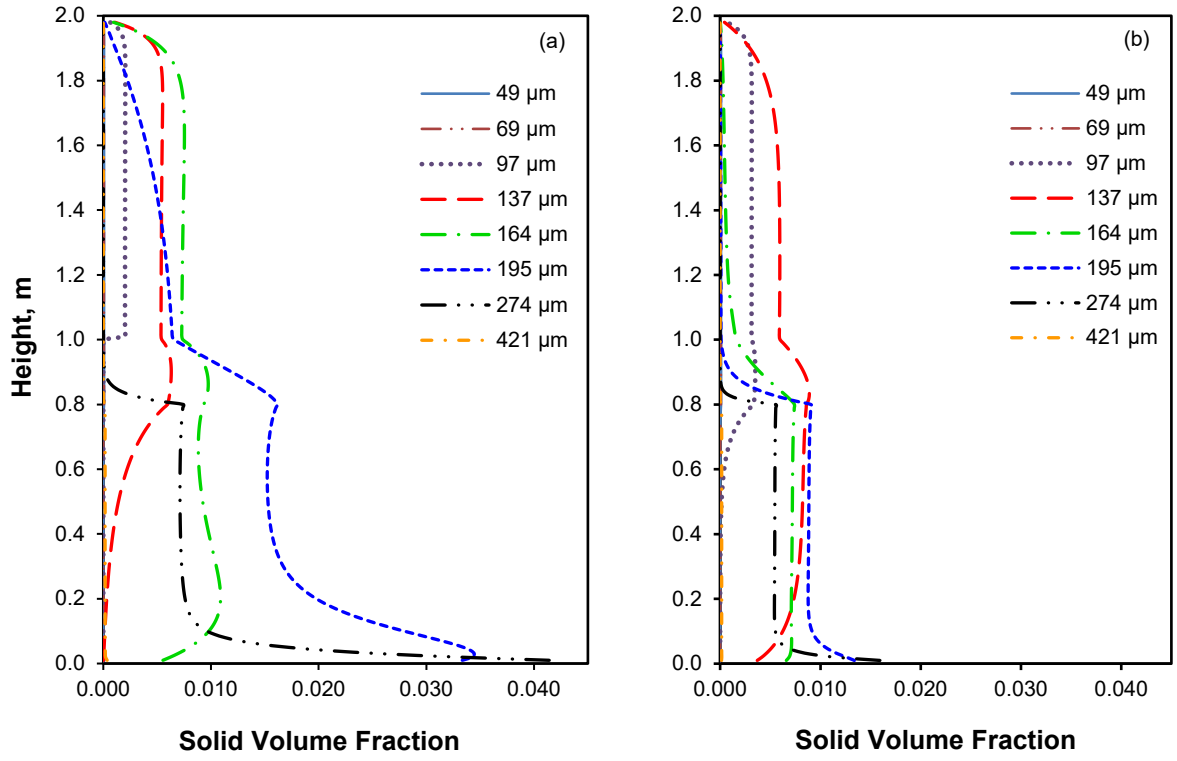

Fig. 8(a-b): Concentration distribution of individual particle species at different underflow rates in element 1: (a) 0.0025 m^3/m^2s; (b) 0.0065 m^3/m^2s.

3.2.5. Influence of solids throughput

Fig. 9 presents the partition number versus particle size at solids throughputs of 0.00030, 0.00042 and 0.0031 m^3/m^2s with underflow rates of 0.0045, 0.0070 and 0.018 m^3/m^2s, respectively. The underflow rate was altered for each new solids throughput to maintain the same d_{50} value and in turn observe the variation in the separation quality, while keeping the fluidization velocity constant at 0.016 m/s. The results show that for the same value of the d_{50} (150 μm) the slope of the partition curves for the higher solids throughput (0.0031 m^3/m^2s) was lower demonstrating that the separation

quality became poorer with increasing throughput. At a higher throughput, the superficial velocity at the feed inlet was higher because a larger quantity of solids with water entered the system.

In Fig. 9, the separation performance of the Reflux Classifier (RC) can also be observed by examining the changes in imperfection with increasing solids throughputs. The imperfection changed from 0.066 to 0.31 with increasing solids throughputs. When the solids throughput was increased from 0.00030 to 0.00042 m^3/m^2s there was a slight decline in the separation quality as the value of imperfection changed from 0.066 to 0.093, showing the capability of the RC to perform well at high throughputs. However, a further significant increase in the solids throughput (0.0031 m^3/m^2s) increased the imperfection to 0.31. This behaviour of the RC predicted by the model was similar to that observed experimentally by Doroodchi et al. (2006). It is also important to note that the RC throughputs are more than three times higher those used for conventional liquid fluidized beds (Galvin et al., 2002; Doroodchi et al., 2006).

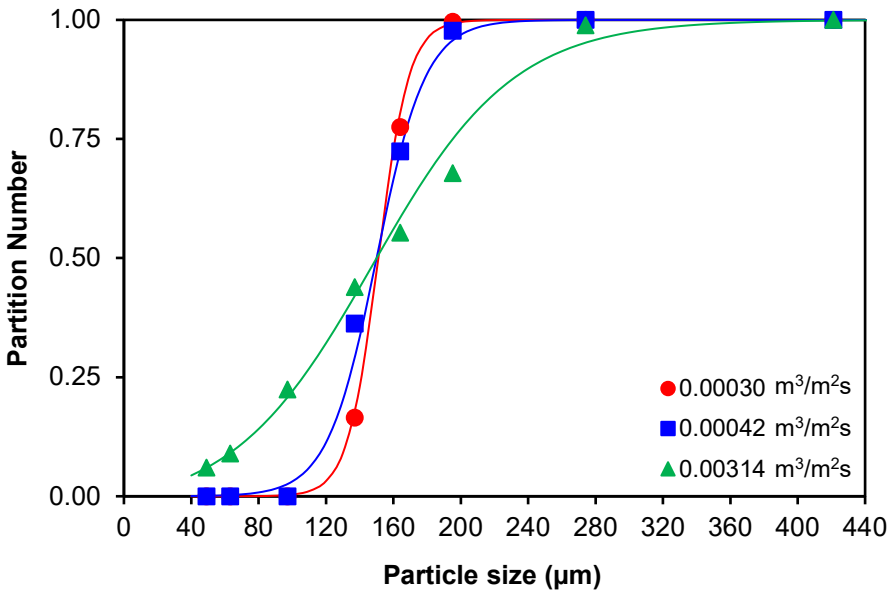

Fig. 9: Partition number versus particle size at solids throughputs 0.00030, 0.00042 and 0.00314 m^3/m^2s with underflow rates 0.0045, 0.0070 and 0.018 m^3/m^2s, respectively.

3.2.6. Concentration distribution at different solids throughputs

Fig. 10a-b shows the concentration distribution of individual particle species versus height at two different solids throughputs, 0.00042 and 0.0031 m^3/m^2s, at steady state conditions. Fig. 10a shows the concentration distribution of individual particle species versus height when the solids throughputs and the underflow rates were 0.00042 and 0.0070 m^3/m^2s, respectively. In this simulation run the concentration profiles are very similar to the cases previously discussed showing the finer species conveying to the overflow while the coarser particles discharged via the underflow. As the value of the d_{50} was 150 μm, the particle species of 137 and 164 μm acted as proxies for the d_{50}, with an elevated presence in both sections of the RC.

Fig. 10b showed a drastic change in the concentration profiles of the particle species when the solids throughput was increased significantly to 0.0031 m^3/m^2s. The scale of the figure has been changed in this case to present the internal state of the system clearly. The results show that the finer and coarsest species (49, 69 and 421 μm) almost completely moved out from the RC. However, high concentrations of the particle species of size between 97 and 274 μm (5 types of species) were observed within the RC. A relatively high underflow rate of 0.018 m^3/m^2s was maintained during the simulations, but the feed flux was so high that the species could not segregate completely, and thus overloaded the system. As a result, the fluidization and inclined sections had higher concentrations of particle species, corresponding to a poorer separation performance.

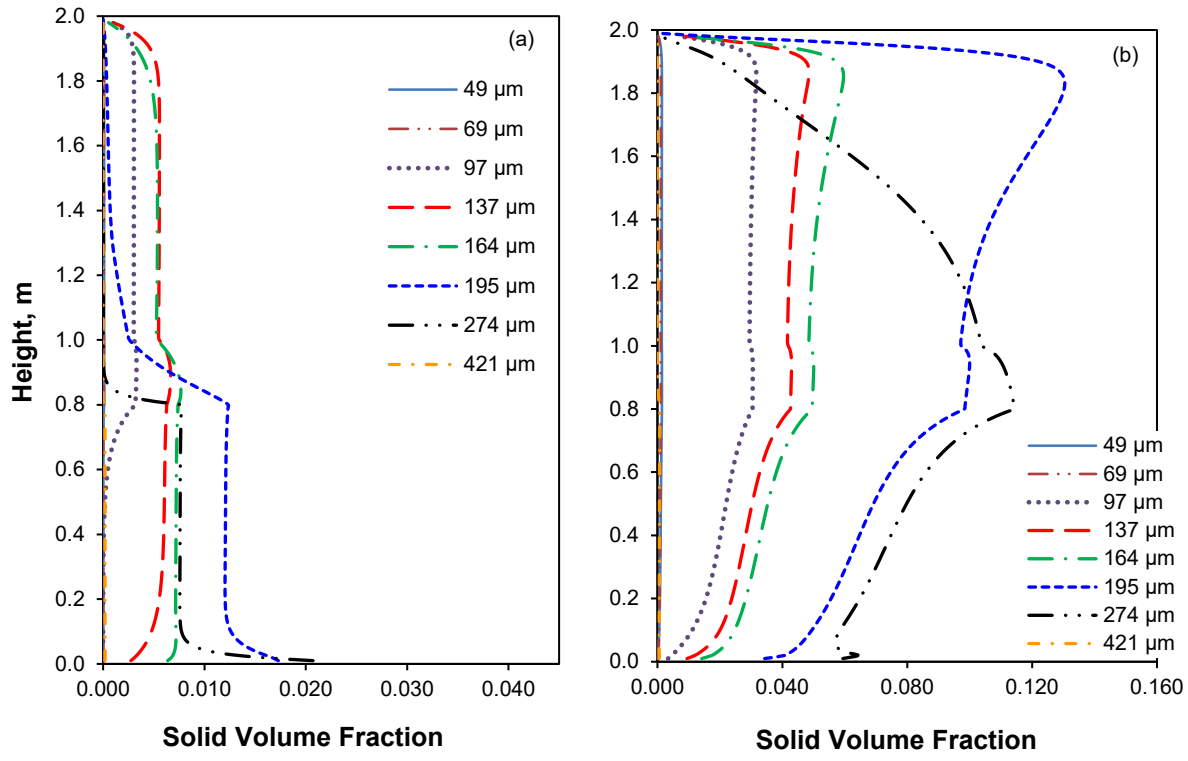

Fig. 10(a-b): Concentration distribution of individual particle species at different solids throughputs in element 1: (a) 0.00042 m^3/m^2s; (b) 0.0031 m^3/m^2s.

Table 3 provides a summary of the results obtained from the simulations. The results show variations in the values of the d_{50} and imperfection, *I*, by altering the fluidization velocity, underflow rate and solids throughput. At a higher fluidization velocity (Run 2) and even at higher underflow rate (Run 4), the separation performance of the device was affected and an increase in the values of the imperfection, *I,* was observed. Similarly, an increase in the solids throughput also decreased the separation performance of the device and a value of *I*, of 0.31 (Run 6) was determined.

Overall, the simulation results obtained in this study, showed that the best results were obtained for Run 1, in which a low fluidization velocity (0.016 m/s), gave a d_{50} value of 150 µm and a lower imperfection value of 0.066.

The theoretical concertation profiles of the particle species generated through model predictions at different operating conditions within the RC were dominated by the particle species of a size close to that of the d_{50}. Basically, the transport of a species is governed by its velocity relative to the container multiplied by its concentration. This transport velocity reduces effectively to near zero for particles having an equal

probability of reporting to the overflow and the underflow, the so-called d_{50}, hence the corresponding concentration of the species must increase disproportionately relative to other species.

Table 3: Summary of simulation runs.

Simulation runs	Fluidization velocity (m/s)	Underflow rate (m^3/m^2s)	Solids throughput (m^3/m^2s)	Imperfection, *I*	Separation size, d_{50} (μm)	Particle species acting as proxies for corresponding d_{50} (μm)
Run 1	0.016	0.0045	0.00030	0.066	150	137 164
Run 2	0.028	0.0045	0.00030	0.071	176	164 195
Run 3	0.016	0.0025	0.00030	0.065	170	164 195
Run 4	0.016	0.0065	0.00030	0.085	130	137
Run 5	0.016	0.0070	0.00042	0.093	150	137 164
Run 6	0.016	0.018	0.0031	0.31	150	overloaded

This paper mainly focused on size classification, whereas the study carried out by Syed et al. (2018) focused on the separation of particle species according to their density. Industrially, the density-based separation method is a challenging proposition where the goal is to partition the lower density particles covering a wide size range to the overflow, and the denser particles over a similarly wide size range to the underflow. Specific separation mechanisms were exploited, notably the fluidized bed inversion phenomenon, and the shear induced hydrodynamic dispersion or inertial lift within the inclined channels. For example, the results obtained by Syed et al. (2018) demonstrated that the particle species of size 1700 μm and density equal to 1275 kg/m^3 having a terminal settling velocity of 0.074 m/s (Syed et al., 2018, Table 1) reported to the overflow (Syed et al., 2018, Fig.4a) despite having a high terminal settling velocity. While, a particle species of size 300 μm and density equal to 2500 kg/m^3 with relatively low terminal settling velocity of 0.035 m/s discharged to the underflow (Syed et al., 2018, Fig.4a).

In the present study, coarser particle species of sizes 274 and 421 μm having terminal settling velocities equal to 0.032 and 0.052 m/s (Table 2), respectively, discharged into

the underflow in all the simulation runs. While the finer particle species with comparatively low terminal settling velocities equal to 0.0019 m/s (49 μm) and 0.0032 m/s (64 μm) transported via the overflow. In the present study, it is illustrated that the movement of the particle species within the RC proceeds according to the particle size.

4. Conclusions

The RC was modelled to investigate the size classification of binary and multicomponent mixtures comprising particle species of density 2490 kg/m^3 using the 2D segregation-dispersion model. The binary mixture consisting of particle species of size 200 and 300 μm was selected for the simulations. It was observed that coarser particle species had a higher concentration near the base, with a maximum concentration of 0.17, whereas the finer particle species had a higher concentration (0.044) in element 1 of the inclined section of the RC. Within the inclined section, the concentration of the finer particle species was higher near the upward facing wall of the channel (element 1), however, it decreased across the channel width from 0.044 to 0.039 as the element number increased from 1 to 21. This was due to the lack of shear lift induced dispersion.

In the second case, simulations were performed under different operating conditions for a multicomponent mixture comprising 8 types of particle species ranging from 49 to 421 μm in size. It was found for the case of the highest fluidization velocity, 0.028 m/s, that most of the species reported to the overflow and the values of the d_{50} and imperfection, *I*, increased from 150 to 176 μm and 0.066 to 0.071, respectively. The partition curves predicted by the 2D model were validated using the published experimental results, achieving very good agreement.

Furthermore, the model predictions obtained for different underflow rates showed a poor separation performance with increasing underflow rate. The imperfection value changed from 0.065 to 0.085 for the underflow rates 0.0025 to 0.0065 m^3/m^{2}s, respectively. Likewise, the study at high solids throughput showed that the separation performance became poor with increasing solids throughput. The imperfection, *I*, value changed from 0.066 to 0.31 when the solids throughput increased from 0.0045 to 0.018 m^3/m^{2}s. It was found that the solids throughput, had a much stronger influence on the separation performance of the RC than the fluidization or underflow rate within the range of values studied.

The 2D segregation-dispersion model was also used to describe the internal state of the system for a multicomponent system for the first time. The concentration profiles of the individual particle species in the fluidization and inclined sections of the RC were demonstrated. The results showed that particle species having sizes closer to the values of the d_{50} segregated at a lower rate relative to the vessel and therefore had a much larger presence within the RC than the other particle species.

Acknowledgements

The authors acknowledge the University of Newcastle Australia and Australian Government RTP scholarship for this PhD research topic. The authors acknowledge the financial support of the Australian Research Council, Australian Coal Association Research Program (ACARP), and FLSmidth.

The University of Newcastle holds international patents on the REFLUX™ Classifier and has a Research and Development Agreement with FLSmidth Pty Ltd. One of the report authors, K. P. Galvin, is the inventor of the REFLUX™ Classifier and is a beneficiary of the University's intellectual property policy.

Appendix A – Concentration profiles

Concentration profile in element 11 and 21

Fig. A.1 shows the concentration profiles of individual particle species for the case 1 of Fig. 5 when the fluidization velocity was kept at 0.016 m/s. The figure shows that overall there is a small difference in the values of the solids concentration in element 1 (Fig. 6a), 11 and 21. This is because, the particle species were mostly being suspended across the channel width due to high fluidization velocity. The superficial velocity with which the fluid (slurry) entered the inclined channel was 0.019 m/s (fluidization + feed - underflow). At this higher superficial fluidization velocity, the fine solid particle species, 49 and 69 μm, moved out from the system in the overflow, whereas the coarser species, ranging from 195 to 421 μm, discharged from the base. However, the solid particle species of size 95 and 137 μm were retained by the RC due to the presence of the inclined channels even though those particles had very low settling velocities (Table 2). Moreover, the suspension mostly consisted of particle species of sizes 137 and 164 μm, close in value to the d_{50}.

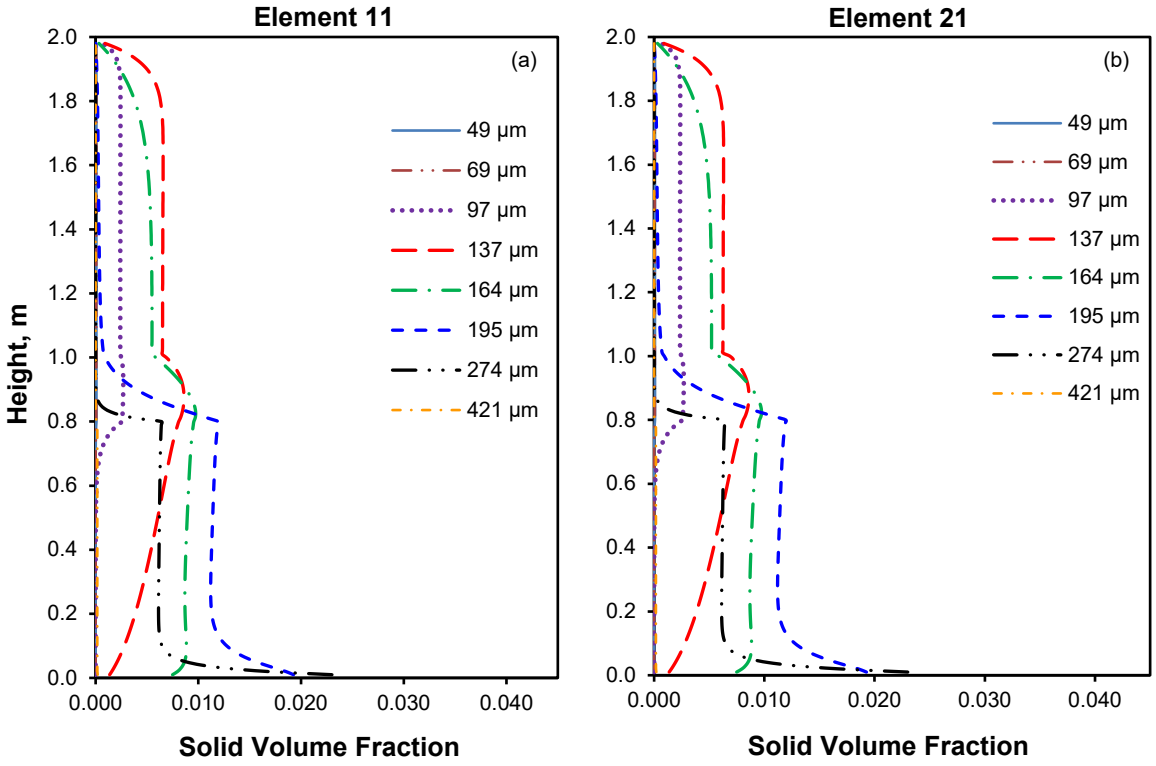

Fig. A.1(a-b): Concentration distribution of individual particle species at a fluidization velocity of 0.016 m/s: (a) element 11; (b) element 21.

Similarly, Fig. A.2 shows the concentration profiles of individual particle species in element 11 and 21 for the case in Fig. 8a when the underflow rate was kept at 0.0025 m^3/m^2s.

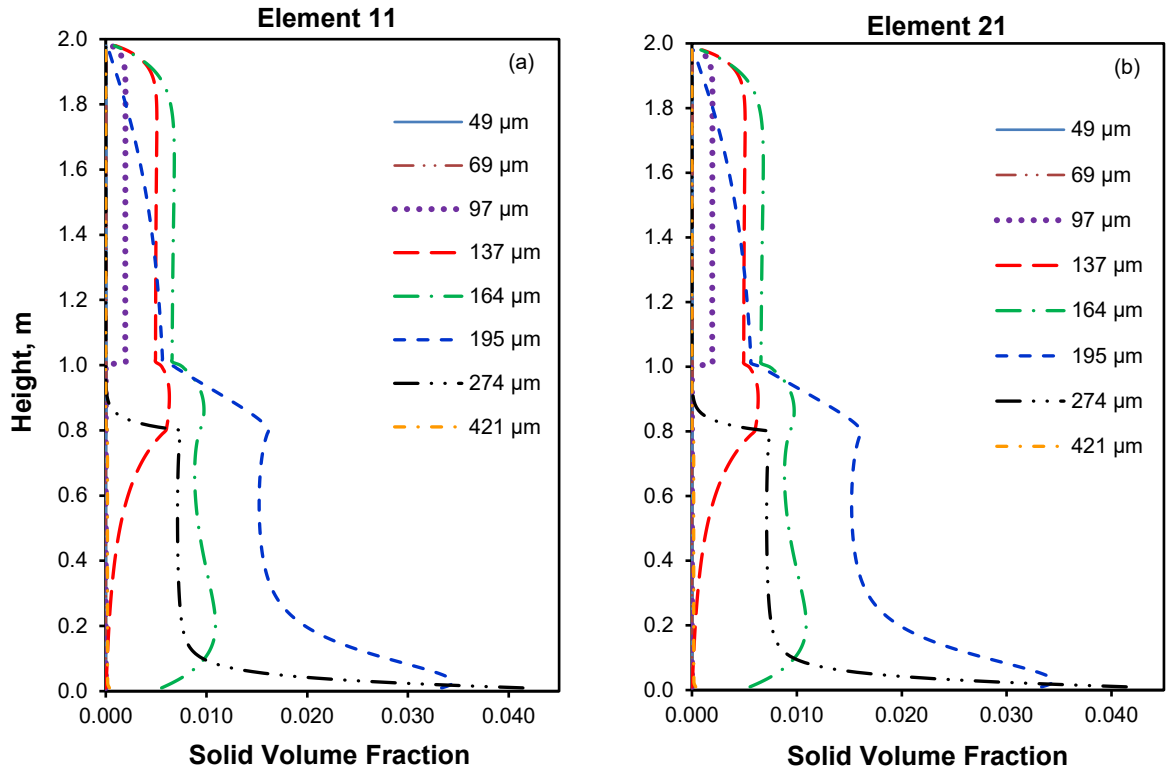

Fig. A.2(a-b): Concentration distribution of individual particle species at an underflow rate 0.0025 m^3/m^2s: (a) element 11; (b) element 21.

References

Amariei, D., Michaud, D., Paquet, G., Lindsay, M., 2014. The use of a Reflux Classifier for iron ores: Assessment of fine particles recovery at pilot scale. Mineral Engineering 62, 66-73.

Anderson, T. B., Jackson, R., 1967. Fluid mechanical description of fluidized beds. Equations of motion. Industrial & Engineering Chemistry Fundamental 6, 527-539.

Asif, M., 1997. Modelling of multi-solid liquid fluidized beds. Chemical Engineering Technology 20, 485-490.

Asif, M., Petersen, J.N., 1993. Particle dispersion in a binary solid–liquid fluidized bed. A.I.Ch.E. Journal 39 (9), 1465-1471.

Boycott, A.E., 1920. Sedimentation of blood corpuscles. Nature 104, 532.

Cornelissen, J.T., Taghipour, F., Escudie, R., Ellis, N., Grace, J.R., 2007. CFD modelling of a liquid–solid fluidized bed. Chemical Engineering Science 62, 6334-6348.

Di Felice, R., 1995. Hydrodynamics of liquid fluidization. Chemical Engineering Science 50, 1213-1245.

Doroodchi, E., Zhou, J., Fletcher, D.F., Galvin, K.P., 2006. Particle size classification in a fluidized bed containing parallel inclined plates. Minerals Engineering 19, 162-171.

Epstein, N., 2005. Teetering. Powder Technology 151, 2-14.

Galvin, K.P., Callen, A., Zhou, J., Doroodchi, E., 2005. Performance of the reflux classifier for gravity separation at full scale. Minerals Engineering 18, 19-24.

Galvin, K.P., Nguyentranlam, G., 2002. Influence of parallel inclined plates on a liquid fluidized bed system. Chemical Engineering Science 57, 1231-1234.

Galvin, K.P., Zhou, J., Walton, K., 2010. Application of closely spaced inclined channels in gravity separation of fine particles. Minerals Engineering 23, 326-338.

Horio, M., 2010. Fluidization science, its development and future. Particuology 8, 514 -524.

Huang, X., 2011. CFD modelling of liquid–solid fluidization: Effect of drag correlation and added mass force. Particuology 9, 441-445

Hunter, D. M., Zhou, J., Iveson, S. M., & Galvin, K. P., 2016. Gravity separation of ultra-fine iron ore in the Reflux Classifier. Mineral Processing and Extractive Metallurgy 125, 126-131.

Juma, A. K. A., Richardson, J.F., 1983. Segregation and mixing in liquid fluidized beds. Chemical Engineering Science 38, 955-967.

Kennedy, S.C., Bretton, R.H., 1966. Axial dispersion of spheres fluidized with liquids. A.I.Ch.E. Journal 12, 24-30.

Khan, M.J.H., Hussain, M.A, Mansourpour, Z., Mostoufi, N., Ghasem, N.M., Abdullah, E.C., 2014. CFD simulation of fluidized bed reactors for polyolefin production – A review. Journal of Industrial and Engineering Chemistry 20, 3919-3946.

Mukherjee, A.K., Mishra, B.K., Kumar, R. V., 2009. Application of liquid/solid fluidization technique in beneficiation of fines. International Journal of Mineral Processing 92, 67-73.

Nguyentranlam, G., Galvin, K.P., 2001. Particle classification in the reflux classifier. Mineral Engineering 14, No. 9, 1081-1091.

Patel, B.K., Ramirez, W.F., Galvin, K.P., 2008. A generalized segregation and dispersion model for liquid fluidized beds. Chemical Engineering Science 63, 1415-1427.

Ramirez, W.F., Galvin, K.P., 2005. Dynamic model of multi-species segregation and dispersion in fluidized beds. AIChE journal 51, 2103-2108.

Rasul, M.G., Rudolph, V., Wang, F.Y. 2000. Particles separation using fluidization techniques. International Journal of Mineral Processing 60, 163-179.

Richardson, J.F., Zaki, W.N., 1954. Sedimentation and fluidization: Part I. Transactions of the Institute of Chemical Engineers 32, 35-53.

Syed, N.H., 2017. A Continuous, Dynamic and Steady State Segregation-Dispersion Model of the Reflux Classifier. PhD Thesis, The University of Newcastle, NSW, Australia.

Syed, N.H., Dickinson, J.E., Galvin, K.P., Moreno-Atanasio, R., 2018. Continuous, dynamic and steady state simulations of the reflux classifier using a segregation-dispersion model. Minerals Engineering 115, 53-67.

Zhu, H.P., Zhou, Z.Y., Yang, R.Y., Yu, A.B., 2008. Discrete particle simulation of particulate systems: A review of major applications and findings. Chemical Engineering Science 63, 5728-5770.

Zigrang, D.J., Sylvester, N.D., 1981. An explicit equation for particle settling velocities in solid–liquid systems. A.I.Ch.E. Journal 27 (6), 1043-1044.